FISEVIER

Contents lists available at ScienceDirect

### **Quaternary Science Reviews**

journal homepage: www.elsevier.com/locate/quascirev



# ENSO effect on hydroclimate changes in southeastern China over the past two millennia



Jianshun Chen <sup>a, b, c</sup>, Kan Zhao <sup>a, b, c, \*</sup>, Yongjin Wang <sup>a, b, c, \*\*</sup>, Yingfang Cui <sup>d</sup>, Yijia Liang <sup>e</sup>, Qingfeng Shao <sup>a, b, c</sup>, Hai Cheng <sup>f, g</sup>, R. Lawrence Edwards <sup>g, a</sup>, Fucai Duan <sup>h</sup>, Shitao Chen <sup>a, b, c</sup>, Chuang Pian <sup>a, b, c</sup>, Junji Zhu <sup>a, b, c</sup>

- <sup>a</sup> School of Geography, Nanjing Normal University, Nanjing 210023, China
- <sup>b</sup> Key Laboratory for Virtual Geographic Environment (Nanjing Normal University), Ministry of Education, Nanjing 210023, China
- Fliangsu Center for Collaborative Innovation in Geographical Information Resource Development and Application, Nanjing 210023, China
- <sup>d</sup> Nanjing Institute of Tourism and Hospitality, Nanjing 211100, China
- <sup>e</sup> College of Geosciences, Nantong University, Nantong, 226007, China
- <sup>f</sup> Institute of Global Environmental Change, Xi'an Jiaotong University, Xi'an 710049, China
- <sup>g</sup> Department of Earth Sciences, University of Minnesota, Minneapolis, MN 55455, USA
- h College of Geography and Environment Sciences, Zhejiang Normal University, Jinhua 321004, China

#### ARTICLE INFO

#### Article history: Received 15 March 2022 Received in revised form 24 April 2022 Accepted 25 April 2022 Available online 5 May 2022

Handling Editor: Dr Mira Matthews

Keywords: EASM Stalagmite ENSO Southeastern China The last two millennia

#### ABSTRACT

Meteorological observations indicate that both natural and anthropogenic forcing contribute to regional drought/flood in the East Asian summer monsoon (EASM) domain. However, spatiotemporal rainfall pattern and its dynamics during natural climatic variability remains unclear. Here we reconstruct a ~3 year-resolution EASM precipitation record over the past two millennia, based on 13  $^{230}$ Th dates and 600  $\delta^{18}$ O in a stalagmite from Songya Cave, southeastern China. The  $\delta^{18}$ O sequence shows a long-term decreasing trend, indicating an increasing monsoon precipitation over the past two millennia. A series of centennial-scale fluctuations are superimposed on the long-term trend, with a wetter Little Ice Age than the Medieval Warm Period. The long-term trend and centennial-scale oscillations in EASM rainfall are broadly related to El Niño-Southern Oscillation (ENSO) and Pacific decadal oscillation (PDO) variations, with an increased (decreased) EASM rainfall corresponding to El Niño-like (La Niña-like) conditions and positive (negative) phase of PDO. Comparison of  $\delta^{18}$ O records from Songya and Wanxiang Cave shows an anti-phased spatial rainfall pattern between southeastern and northwestern China. This spatiotemporal rainfall pattern, consistent with the modern observations, is possibly regulated by the ENSO, through changes in the location and strength of the Western Pacific Subtropical High (WPSH).

© 2022 Elsevier Ltd. All rights reserved.

#### 1. Introduction

The hydroclimate of East Asia is mainly controlled by the East Asian summer monsoon (EASM), which transports humid moistures from the marine source to the interior of the East Asian continent. Advance or retreat of the monsoon circulation could lead to either deficient or excessive precipitation, which substantially affect the economy and society of the region (Cook et al., 2010;

E-mail addresses: 09371@njnu.edu.cn (K. Zhao), yjwang@njnu.edu.cn (Y. Wang).

Zhang et al., 2021a). Clarifying the natural rhythm and forcing mechanism of the EASM is important to projection of future precipitation within the context of anthropogenic global warming.

Paleoclimate records spanning the past two millennia are often characterized as a warm Medieval Warm Period (MWP, ~950-1300 AD) between cool Dark Age Cold Period (DACP, ~400-900 AD) and Little Ice Age (LIA, ~1400-1850 AD) (Lamb, 1965; Mann et al., 2009). The "south-north" dipolar pattern of precipitation on centennial timescale in monsoon-dominated eastern China (monsoonal China, area approximately east of 105°E) has been substantiated by integrated paleoclimate proxies which record the moisture and/or precipitation variations (Chen et al., 2015). The dipolar pattern behaves as "droughts in the south and floods in the north" during the MWP and "floods in the south and droughts in the north"

 $<sup>^{*}</sup>$  Corresponding author. School of Geography, Nanjing Normal University, Nanjing, 210097, China.

<sup>\*\*</sup> Corresponding author. School of Geography, Nanjing Normal University, Nanjing 210023. China.

during the DACP and LIA, probably linked to changes in Northern Hemisphere temperature and/or sea surface temperatures (SSTs) in tropical Pacific Ocean (Chen et al., 2015; Zhao et al., 2020). A tripolar rainfall pattern was also proposed by meteorological observations (Ding et al., 2008; Chiang et al., 2017) and paleoclimatic studies (Chiang et al., 2015). One phase of this tripolar pattern is characterized by droughts in northern and southern China, but floods in central China (Chiang et al., 2015, 2017), which is mainly associated with the duration of Meiyu and the zonal movement of westerlies. A recent pollen study at Xinjie site from the lower Yangtze region show that the rainfall pattern concurs with stalagmite and other proxy records from southern China but differs from proxy records in northern China (Lu et al., 2019). Moreover, hydroclimate variations inferred from Lake Nvshan sediments in the Jiang-Huai region of eastern China indicate that rainfall in the lower Yangtze region was higher during the LIA than during the MWP (Jiang et al., 2021). However, a composite high-resolution monsoon rainfall record inferred from stalagmites in three caves over the middle Yangtze Valley shows a wet condition in the MWP and dry conditions in the DACP and LIA (Zhang et al., 2021b), in consistent with the palaeohydrological reconstruction from Poyang Lake (Yao et al., 2015). Therefore, there are controversial views about the hydroclimate state and spatial rainfall pattern over the past two millennia in monsoonal China.

Observational and modelling evidence indicate that not only external forcing, but also internal climate variability, contributed substantially to the EASM change and spatial rainfall pattern over the past two millennia (Masson-Delmotte et al., 2013). For example, decreased (increased) monsoon rainfall during the LIA (MWP) was associated with low (high) solar irradiance and high (low)

atmospheric aerosol concentrations as a result of volcanic eruptions (Zhang et al., 2008). In addition, the El Niño-Southern Oscillation (ENSO), Pacific decadal oscillation (PDO) and/or Atlantic multidecadal oscillation (AMO) have been also suggested to impact the hydroclimate variability and spatial distribution of rainfall in the EASM domain by altering the position and strength of the Western Pacific Subtropical High (WPSH) and the westerly jet (Chiang et al., 2015, 2017; Jiang et al., 2021; Zhang et al., 2021b). Therefore, uncertainties remain in the history and driving mechanisms of the EASM variability and associated spatial rainfall pattern over the past two millennia, partly due to the scarcity of high-quality hydroclimate records in the EASM domain.

Here, we present a ~3 year-resolution stalagmite  $\delta^{18}$ O record from Songya Cave in southeastern China to reconstruct the history of EASM precipitation over the past two millennia. Our study has two aspects: (1) exploring the behavior of precipitation variability in southeastern China over the past two millennia and (2) clarifying the spatiotemporal rainfall pattern in monsoonal China and its forcing mechanism.

#### 2. Material and methods

Songya Cave (29°10′N, 119°40′E; 668 m above sea level) is located in Mt. Jinhua, Zhejiang Province, southeastern China (Fig. 1). Modern observational data from Jinhua meteorological observatory shows that the mean annual temperature and precipitation are ~18 °C and ~1424 mm, respectively. Local precipitation increases in late spring as the EASM intensifies (Ding and Chan, 2005). The annual precipitation ranges from 990 mm to 1900 mm, with ~54% occurring during summer (May—September). The variability of the

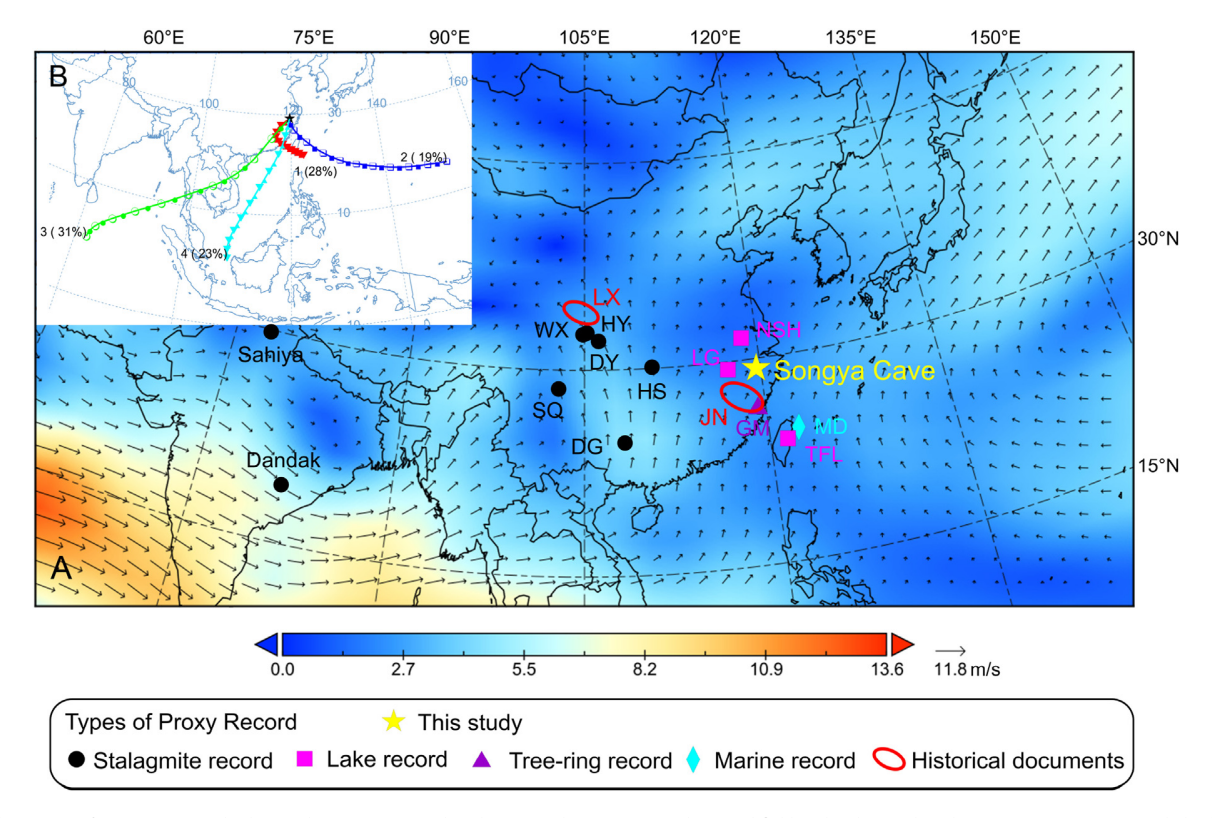


Fig. 1. (A) Location of Songya Cave and other study sites mentioned in the text and May to September wind field under the 850 hPa during 1948—2019 AD. Detailed information about these study sites can be found in Table 1. The arrows represent the air flow direction and the shadow indicates the wind velocity (m/s). The wind field was generated by NCEP/NCAR reanalysis datasets (https://www.esrl.noaa.gov/psd/cgi-bin/data/getpage.pl). (B) The moisture backward trajectories of Songya Cave were computed for the low-level wind parcels at 1500 m (above ground level) for a time period of 240 h at 6-h intervals (May to September 1986—2006) in HYSPLIT version 5.0 (Hybrid Single-Particle Lagrangian Integrated Trajectory model, Draxler and Hess, 1998).

annual rainfall is highly correlated with summer precipitation  $(r^2 = 0.77)$ , but not with rainfall during the rest of the year  $(r^2 = 0.31, Fig. S1)$ . Multi-year mean air mass backward trajectories at the study site show that ~47% of the water vapor is derived from the tropical western Pacific (Fig. 1B), transported by the EASM (Zhou and Yu, 2005). Therefore, regional hydroclimate is prominently influenced by the EASM rainfall (Ding and Chan, 2005). The overlying flora is composed mainly of deciduous herbs. The cave is ~800 m long, and the spacious entrance of cave is connected to the cave chamber along a 300-m narrow passage. The cave is poorly ventilated, and temperature and relative humidity at the time of sample collection (June 2018) were ~17.2 °C and ~100%, respectively. The thin overlying carbonate bedrock results in a weakened smoothing effect of the water reservoir in the karst system (Duan et al., 2016), thus the stalagmite (SY6)  $\delta^{18}$ O could effectively inherits the signal of precipitation  $\delta^{18}$ O.

The stalagmite SY6 was collected on the slope ~700 m from the cave entrance, with a length of ~356 mm and a diameter of ~60 mm. When halved and polished, lithological changes (clays and calcite) and macroscopical hiatus are evident below the depth of 310 mm from the top of SY6 (Fig. 2a). Thus, the upper 300 mm section of SY6 was used in this study. Thirteen subsamples were collected for U—Th dating along the growth axis with a carbide dental drill. <sup>230</sup>Th dating was performed on a multi-collector inductively coupled plasma mass spectrometer (MC-ICP-MS) at the Isotope Laboratory of Nanjing Normal University. The procedures for chemical

separation and purification of uranium and thorium were described in Shao et al. (2017). Six hundred sub-samples for stable isotopic measurement were drilled every 0.5 mm along the growth axis using a carbide dental drill. Stable isotope analyses were performed on a Finnegan MAT 253 mass spectrometer at the Isotope Laboratory of Nanjing Normal University. All isotope values were reported in per mil (‰) relative to Vienna Pee Dee Belemnite (VPDB) standard. The precision is within 0.06‰ for  $\delta^{18}\text{O}$  and 0.05‰ for  $\delta^{13}\text{C}$  at the  $1\sigma$  level.

#### 3. Results

#### 3.1. Chronology

Thirteen  $^{230}\text{Th}$  dating results are shown in Table S1. The  $^{238}\text{U}$  concentrations range from  $2591.2\pm2.4$  to  $5059.6\pm1.9$  ppb and the  $^{232}\text{Th}$  concentrations range from  $6.4\pm0.05$  to  $36.7\pm0.08$  ppb (Table S1). The  $^{230}\text{Th}/^{232}\text{Th}$  activity ratios are low, from  $2.4\pm0.05$  to  $23.0\pm0.14$ , leading to initial detrital  $^{230}\text{Th}$  corrections of 39-229 yr. All ages are in stratigraphic order and the dating errors are within  $\pm20$  to  $\pm114$  yr ( $2\sigma$ ). The stalagmite SY6 age model was constructed using MOD-AGE by LOESS fitting method (Hercman and Pawlak, 2012). The time series was established on the scale of the distance from the base, with 0.5 model resolution. The SPAN factor is automatic and model-derived. The age model shows that the upper 300 mm of stalagmite SY6 grew from 175 to 1840 AD (Fig. 2).

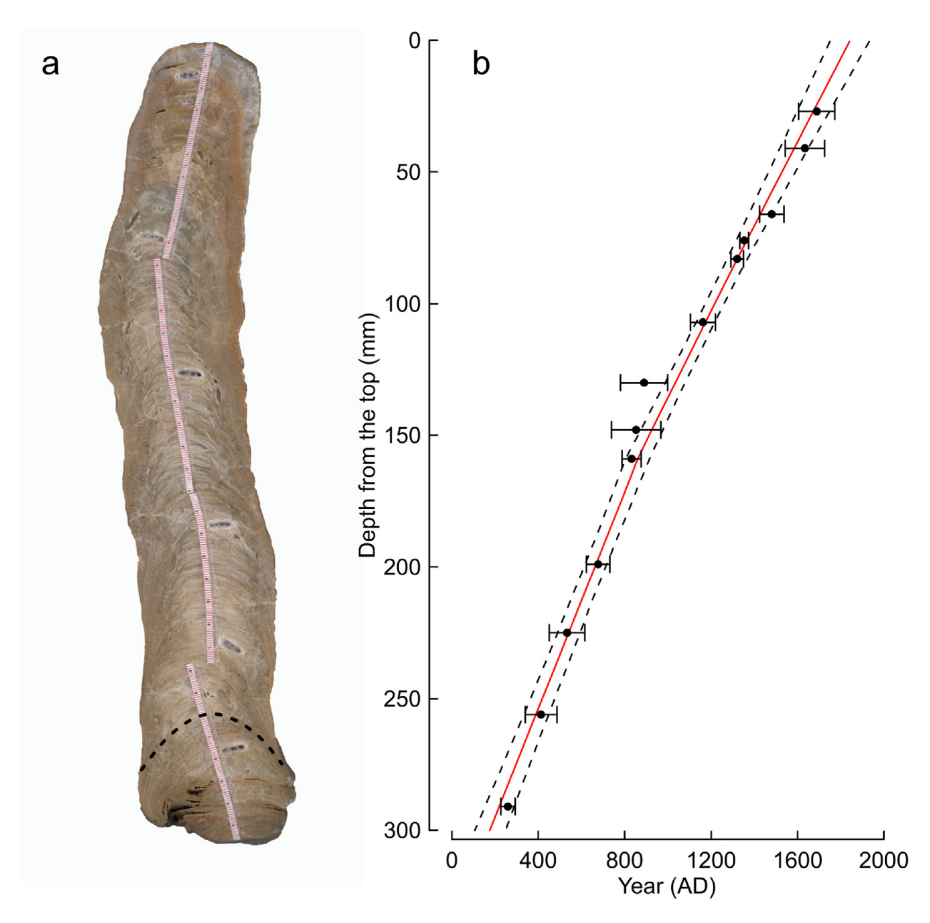


**Fig. 2.** The polished profile (a) and the age model (b) of stalagmite SY6. (a) The black dashed line indicates the location of 300 mm from the top. (b) The age model was constructed by using MOD-AGE (Hercman and Pawlak, 2012). The black dots and horizontal error bars represent  $^{230}$ Th dates and dating errors (within  $2\sigma$  errors), respectively. The red solid line indicates the depth-age model of stalagmite SY6 accompanied with confidence bands (black dashed lines). (For interpretation of the references to color in this figure legend, the reader is referred to the Web version of this article.)

#### 3.2. Stable isotope record

The SY6  $\delta^{18}$ O values fluctuate from -8.17% to -6.53%, with an average value of -7.28%. The  $\delta^{18}$ O record, with an average temporal resolution of  $\sim$ 3 years, shows a long-term decreasing trend (Fig. 3a), until a significant shift to increasing values during 1760 and 1840 AD. Besides, there are a series of centennial-scale oscillations superimposed on the long-term trend. One distinct positive shift is centered at  $\sim$ 750 AD with an amplitude of  $\sim$ 1‰, lasting nearly 100 years.

Stalagmite deposition under isotopic equilibrium fractionation is an important prerequisite for stalagmite  $\delta^{18}O$  as a climate indicator. The Hendy Test (Hendy, 1971) was performed on four single growth laminae at the depth of 35 mm, 170 mm, 210 mm and 240 mm. The results show that the fluctuation of  $\delta^{18}O$  and  $\delta^{13}C$  values along the same growth layer are small, with standard deviations less than 0.2 and 0.25, respectively (Fig. S2a). Moreover, the correlation between  $\delta^{18}O$  and  $\delta^{13}C$  values is statistically insignificant ( $r^2=0.02,\ n=600;\ Fig.\ S2b)$ , suggesting that the stalagmite SY6 was deposited close to isotopic equilibrium condition.

#### 4. Discussion

#### 4.1. Interpretation of stalagmite oxygen isotope record

On orbital and millennial timescales, the continental-scale resemblance of stalagmite  $\delta^{18}O$  records in China indicates the spatially integrated monsoon precipitation between the tropical moisture source and the cave site and/or summer monsoon rainfall in the cave region (Cheng et al., 2016). However, on centennial to decadal timescales, regional differences in Chinese  $\delta^{18}$ O records are evident (Zhao et al., 2020). These  $\delta^{18}$ O records have been interpreted as a result of the monsoon precipitation amount in northern China (Zhang et al., 2008; Tan et al., 2011), the circulation effect in central China (Tan, 2014), and/or the residual ratio of the moisture transport from ocean source to the cave site (Hu et al., 2008). In meteorological studies, many processes were suggested to affect variations in precipitation  $\delta^{18}O$  (Dayem et al., 2010), including different moisture source, different moisture transmission pathway, different condensation and evaporation process within the atmosphere, different types of precipitation and the "circulation effect" (Dayem et al., 2010; Tan, 2014).

Here, we indicate that changes in EASM rainfall mainly control the stalagmite  $\delta^{18}$ O variations in Songya Cave, with lighter (heavier)  $\delta^{18}$ O values corresponding to more (less) EASM rainfall. Firstly, the summer (May-September) precipitation amount data during the period 1979-2009AD are compared to simulated amount-weighted average annual precipitation  $\delta^{18}$ O values of Jinhua City (num: x065y063, 29.523°N, 120°E) (Yoshimura et al., 2008; Fig. S3). All data were obtained from Jinhua meteorological observatory (29°07′N, 119°39′E; 626 mm above sea level) near Songya Cave. Changes in amount-weighted average annual precipitation  $\delta^{18}$ O data are consistent with the EASM rainfall changes, with a correlation coefficient of -0.61 (n = 31, p < 0.01). Cave  $\delta^{18}$ O largely inherits the weighted average annual precipitation  $\delta^{18}$ O signal (Duan et al., 2016), thus reflects the EASM precipitation changes. Secondly, we compared the SY6  $\delta^{18}$ O record with other paleo-rainfall records from the southeastern China (Fig. 3b-d). As shown in Fig. 3b, fluctuations in SY6  $\delta^{18}$ O bear a similarity to changes in the Kuroshio Current (KC) species abundance from the core MD05-2908, with lower  $\delta^{18}$ O values corresponding to lower KC species. The lower KC species is accompanied by lower summer sea-surface salinity, indicating more EASM precipitation (Li et al., 2011). Likewise, our SY6  $\delta^{18}$ O record is compared with the reconstructed paleo-rainfall records from Longan Lake (Fig. 3c, Tong et al., 1997) and Tsuifong

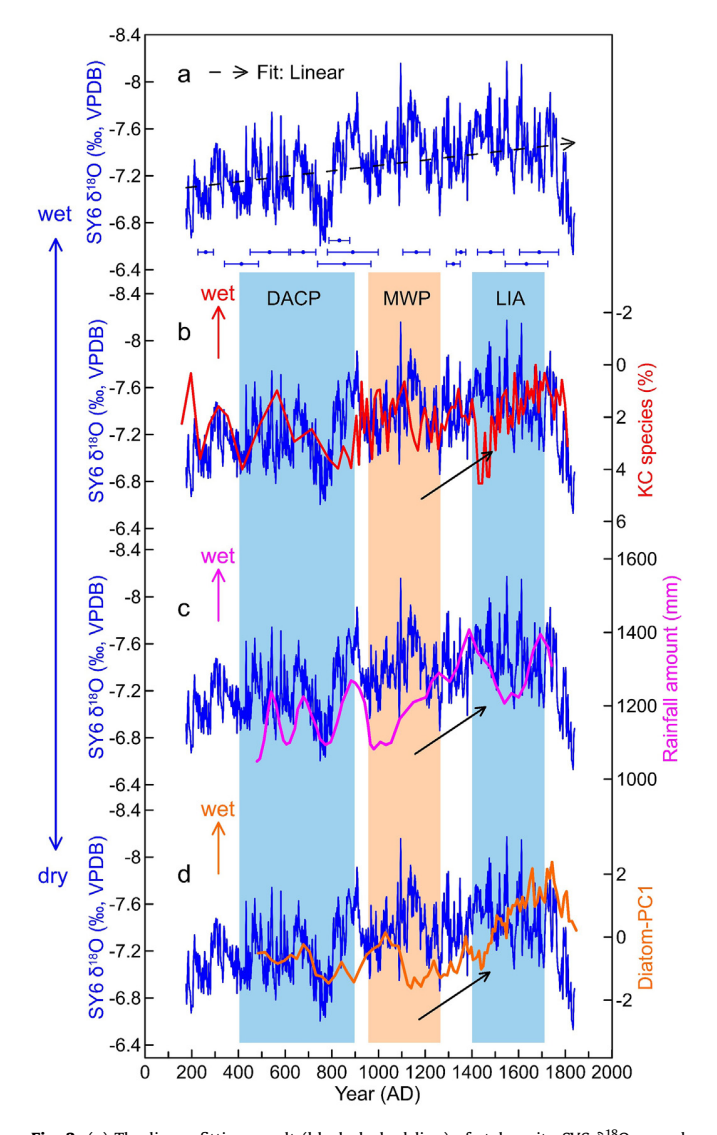


**Fig. 3.** (a) The linear fitting result (black dashed line) of stalagmite SY6  $\delta^{18}$ O record (blue line, this study). The  $^{230}$ Th ages are plotted with 2σ error bars. Comparison among SY6  $\delta^{18}$ O record (blue line), the Kuroshio Current species of the MD05-2908 (b, red line, Li et al., 2011), the pollen record of Longgan Lake (c, pink line, Tong et al., 1997), and the diatom record of Tsuifong Lake (d, orange line, Wang et al., 2013). The black dashed arrow line of SY6  $\delta^{18}$ O represents the long-term trend of EASM rainfall during the last two millennia. The black solid arrow lines indicate that the monsoonal rainfall continuously increased in southeastern China from the MWP to the LIA. The DACP is marked by blue box. The intervals best defining the MWP and LIA based on the NH hemispheric mean series (Mann et al., 2009) are shown by orange and blue boxes, respectively. (For interpretation of the references to color in this figure legend, the reader is referred to the Web version of this article.)

Lake (Fig. 3d, Wang et al., 2013), respectively. The long-term trends in increasing rainfall inferred from the Longgan Lake and Tsuifong Lake, are generally coherent with the decreasing SY6  $\delta^{18}O$  trend over the past two millennia. Historical drought/flood index in southeastern China also displays a wetter trend from the MWP to the LIA (Zheng et al., 2006). Apart from the monsoon-intensity-related rainfall, different moisture sources (adjacent Pacific Ocean or remote Indian Ocean) could also affect the stalagmite  $\delta^{18}O$  values (Tan, 2014). At Songya Cave site, ~70% of the total water vapor is derived from the tropical western Pacific and South China Sea (Fig. 1B). Due to more water vapor coming from the adjacent Pacific Oceans, the lighter SY6  $\delta^{18}O$  is more likely caused by the increased

EASM rainfall. Therefore, the SY6  $\delta^{18}$ O record primarily reflects the EASM rainfall changes in southeastern China, with lighter (heavier)  $\delta^{18}$ O values coincided with increased (decreased) EASM rainfall, and vice versa.

## 4.2. Monsoon rainfall variability and its dynamics in southeastern China

The SY6  $\delta^{18}$ O record indicates a gradually increasing EASM precipitation in southeastern China over the past two millennia, superimposed by several centennial-scale fluctuations (Fig. 3a). Due to age uncertainties in our reconstruction (~65 yr on average), however, we focus on the variations of the low-frequency (long term trend and centennial-scale fluctuations) component in SY6  $\delta^{18}$ O record. The most prominent feature is that the LIA was a relatively humid period in southeastern China, compared with the MWP. This observation is also revealed by other paleo-rainfall records from southeastern China (Fig. 3b-d). For the purpose of investigating the dynamic mechanism, the LIA and MWP were defined distinct three-century-long intervals (1400-1700 AD and 950 to 1250 AD, respectively, as defined by Mann et al., 2009, Fig. 3), which both correspond to relative cold and warm hemispheric conditions and are distinct with regard to the external radiative forcing and internal climate variability (Mann et al., 2009).

In previous studies, the regional hydroclimate changes in southeastern China were related to the modulation of the tropical Pacific Ocean (Cui et al., 2018; Jiang et al., 2021). We compared the SY6  $\delta^{18}$ O record with the sea surface temperature (SST) anomaly in Niño3 region (Mann et al., 2009). The SY6 record is broadly similar to the ENSO record at both long-term trend and centennial-scale

variations (Fig. 4a), indicating that the increasing (decreasing) EASM rainfall is related to the El Niño-like (La Niña-like) conditions. Due to the different temporal resolution between our  $\delta^{18}$ O record (~3 yr) and the tropical SST data (~1 yr), we interpolated the two records to produce a uniform 5-yr spacing and then calculated the correlation coefficient between them. The correlation coefficient is -0.49 during the interval of 900-1750AD (n = 166, p < 0.01, 11-point running mean). In addition, comparison of the SY6  $\delta^{18}$ O record and other ENSO reconstructions shows similar relations between ENSO and EASM rainfall in southeastern China (Conroy et al., 2009; Atwood and Sachs, 2014; Fig. S4). The cause of the decreasing EASM rainfall since 1750 AD (approximately lasting 90 years without  $^{230}$ Th date control) is not clear, partly due to the age uncertainties, and may be correlated with a decadal-scale La Nina-like condition (Atwood and Sachs, 2014; Rustic et al., 2015).

The Pacific Decadal Oscillation (PDO) is a long-lived ENSO-like pattern of Pacific climate variability (Mantua et al., 1997) and has considerable influence on climate in the pan-Pacific basin (Dong and Dai, 2015; Fang et al., 2019). Hence, the SY6 record is further compared to the PDO reconstruction. The variation of EASM rainfall is highly correlated with the SST anomaly over the North Pacific region (22.5°N-57.5°N, 152.5°E–132.5°W) (Mann et al., 2009, Fig. 4b). The long-term trend and centennial-scale oscillations in the two records are comparable. The correlation coefficient is -0.59 (n = 166, p < 0.01, interpolated to a uniform 5-yr spacing and 11-point running mean of the two records). Our SY6 record is also broadly similar to a PDO index based on hydrologically sensitive Pinus flexilis tree-ring chronologies from California and Alberta (MacDonald and Case, 2005; Fig. S4), with a correlation coefficient of -0.24 (n = 147, p < 0.01, interpolated to a uniform 5-yr spacing

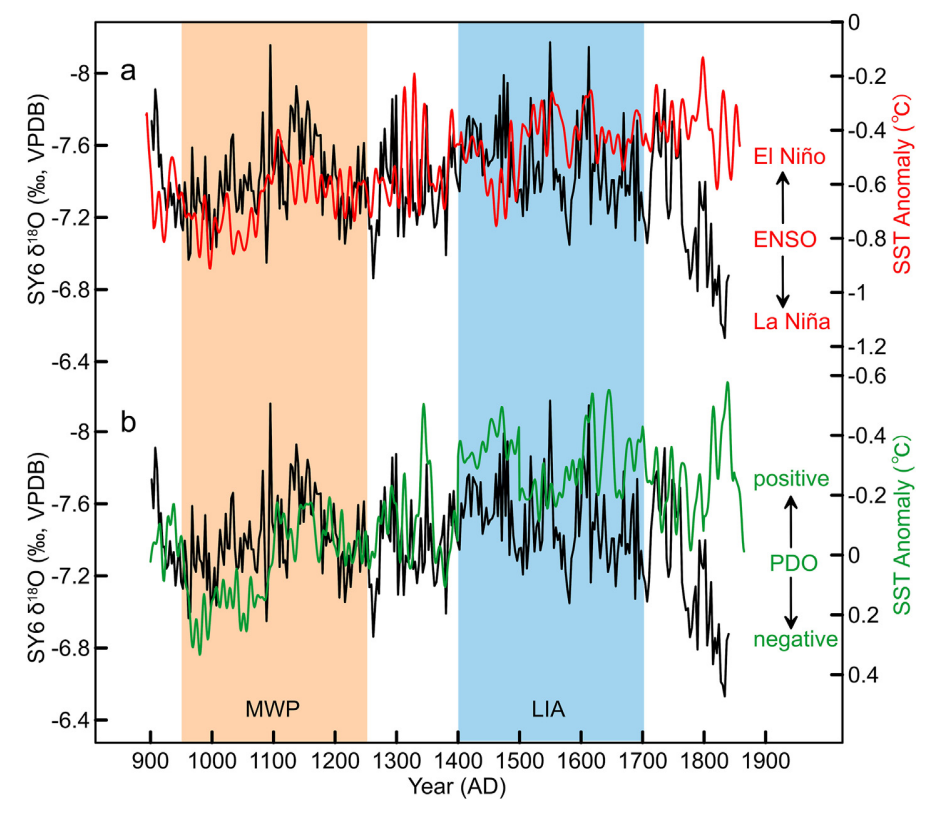


**Fig. 4.** (a) The comparison of stalagmite SY6  $\delta^{18}$ O record (black line) and Niño3 region SST anomaly (11-point smoothing, red line, Mann et al., 2009). (b) The comparison of stalagmite SY6  $\delta^{18}$ O record (black line) and SST anomaly over the central North Pacific region (green line, Mann et al., 2009). The intervals best defining the MWP and LIA based on the NH hemispheric mean series (Mann et al., 2009) are shown by orange and blue boxes, respectively. (For interpretation of the references to color in this figure legend, the reader is referred to the Web version of this article.)

and 11-point running mean). These observations suggest that EASM rainfall in southeastern China is likely related to the PDO, with an increased (decreased) rainfall corresponding to the positive (negative) phase of PDO.

Our observations are consistent with meteorological observations and modelling studies of the relationship between the ENSO, PDO and the EASM precipitation (Ding et al., 2009; Yang et al., 2017). Changes in ENSO and PDO can affect the strength and location of the WPSH and regulate the movement and residence time of the EASM rain belt (Chang et al., 2000; Ding et al., 2009; Yang et al., 2017). During the El Niño-like condition and positive phase of PDO, the enhanced and southward WPSH causes more water vapor to gather in the northwestern flank of the WPSH, where Songya Cave located. The EASM rain belt maintains in southeastern China and contributes more rainfall amount in this region. In contrast, during the La Nina-like condition and negative phase of PDO, the weakened and northeastward shift in WPSH results in the Summer Drought over southeastern China, where the WPSH is overhead. Then, more monsoon moisture from Indian Ocean can penetrate deeply into the northern China, with more rainfall delivered into the EASM limit regions (Zhou and Yu, 2005; Matsumura and Horinouchi, 2016; Yang et al., 2017).

#### 4.3. Spatial rainfall distribution in the EASM domain

East Asia mainly has three branches of tropical water vapor transport for normal climatological conditions: the first is the strong transport by the Indian summer monsoon (ISM), which is linked to the robust cross-equatorial airflows and brings abundant moisture from Indian Ocean, crossing the Indochina Peninsula and the South China Sea northward into eastern China; the second is the transport by the EASM, which comes from the western Pacific and brings moisture from the tropical Pacific Ocean westward into eastern China; The third is the cross-equator flows straddling 105°E-150°E, which is the weakest one among these three branches (Zhou and Yu, 2005). The differences in spatial rainfall pattern in eastern China have been substantiated by instrumental data (Ding et al., 2008) and paleoclimatic records (Chen et al., 2015). The "south-north" dipole pattern of precipitation has been extensively studied (Chen et al., 2015; Zhao et al., 2020). This spatial pattern is probably related to the northward transport of water vapor from the Indian ocean via cross-equatorial airflows (Zhao et al., 2020). Alternatively, the spatial rainfall pattern, modulated by the westward moisture transport from tropical western Pacific though the EASM circulation, remain unclear.

As shown in Fig. 5, the temporal evolution of the SY6  $\delta^{18}$ O record is similar to that of a high-resolution stalagmite record (WX42B) in Wanxiang Cave from northwestern China, but in the opposite sense. The correlation coefficient between them is -0.47 (n = 540, p < 0.01, interpolated to a uniform 5-yr spacing and 11-point running mean). The WX42B  $\delta^{18}$ O record exhibits strong similarity to the regional precipitation records from meteorological observatory and historical drought/flood index, reflecting changes in monsoon rainfall amount (Zhang et al., 2008). Therefore, comparison of  $\delta^{18}$ O records from Songya and Wanxiang Cave indicates a dipole rainfall pattern between southeastern and northwestern China. The multi-centennial scale oscillations in both records are also comparable, but with an inverse relationship. During the DACP, the monsoon rainfall gradually increased in southeastern China, but decreased in northwestern China. From the MWP to the LIA, the monsoon rainfall continuously increased in southeastern China, while northwestern China became drier (Fig. 5). Comparison of other paleo-rainfall records from southeastern (this study, Jiang et al., 2021; Wang et al., 2013; Tong et al., 1997) and northwestern China (Zhang et al., 2008; Tan et al., 2008, 2011) confirms a

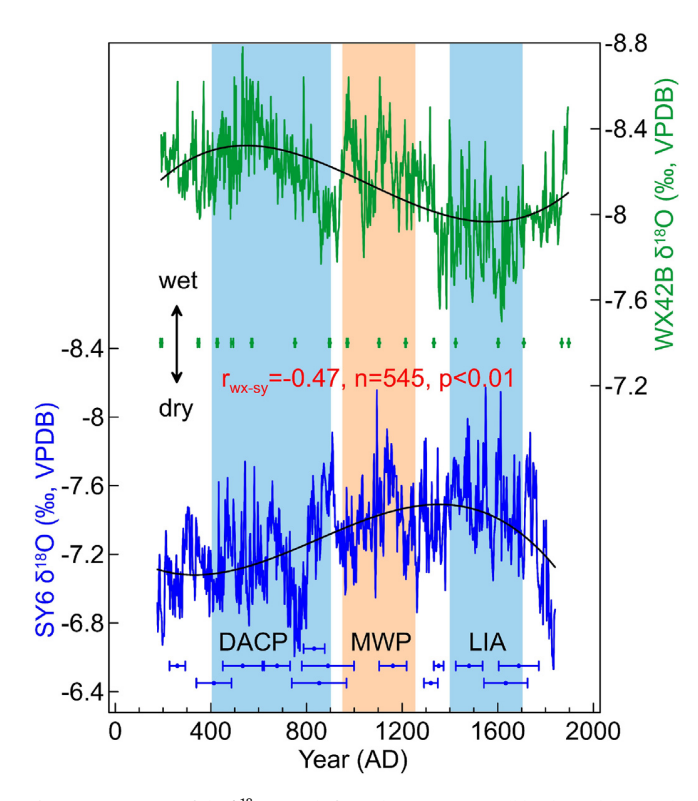


**Fig. 5.** Comparison of the  $\delta^{18}$ O records for stalagmite WX42B (blue line, Zhang et al., 2008) and stalagmite SY6 (green line, this study). The black lines indicate the results of 3rd order polynomial fitting. The age errors  $(2\sigma)$  are color-coded by stalagmites. The DACP is marked by blue box. The intervals best defining the MWP and LIA based on the NH hemispheric mean series (Mann et al., 2009) are shown by orange and blue boxes, respectively. (For interpretation of the references to color in this figure legend, the reader is referred to the Web version of this article.)

long-term increasing monsoon rainfall in southeastern China and a long-term decreasing monsoon rainfall in northwestern China over the past two millennia (Fig. 6A). A recent study also revealed an opposite rainfall pattern between Xinjie site (southeastern China, ~244 km north of Songya Cave) and Gonghai Lake (northern China) during the late Holocene (Lu et al., 2019). Therefore, these observations demonstrate a "southeastern-northwestern" diploe pattern of precipitation in eastern China on the long-term trend and multicentennial timescale, consistent with the longitudinal zonality in EASM rainfall pattern.

Furthermore, the "southeastern-northwestern" diploe rainfall pattern is probably modulated by the ENSO. Comparison of ENSO index and WX42B  $\delta^{18}$ O record shows that the ENSO-rainfall relationship is also evident in northwestern China (r = 0.66, n = 181, p < 0.01, interpolated to a uniform 5-yr spacing and 11-point running mean; Fig. S5), but in a sense opposite to that in southeastern China. Lighter (heavier)  $\delta^{18}$ O values, corresponding to higher (lower) monsoon rainfall in northwestern China, are related to the La Niña-like (El Niño-like) condition. Other paleo-rainfall records from southeastern and northwestern China also confirms the relationship between ENSO and spatial rainfall pattern (Cui et al., 2018; Jiang et al., 2021; Lu et al., 2019). These observations are consistent with meteorological studies of the relationship between ENSO and spatial rainfall pattern, showing an anti-phased rainfall pattern between northwestern and southeastern China related to the enhanced El Niño during 1950-2018AD (Fig. 6B). Moreover, summer precipitation anomalies (May to October) in the southeastern China also display various degrees of inversed correlation with other monsoonal regions in the El Niño years during

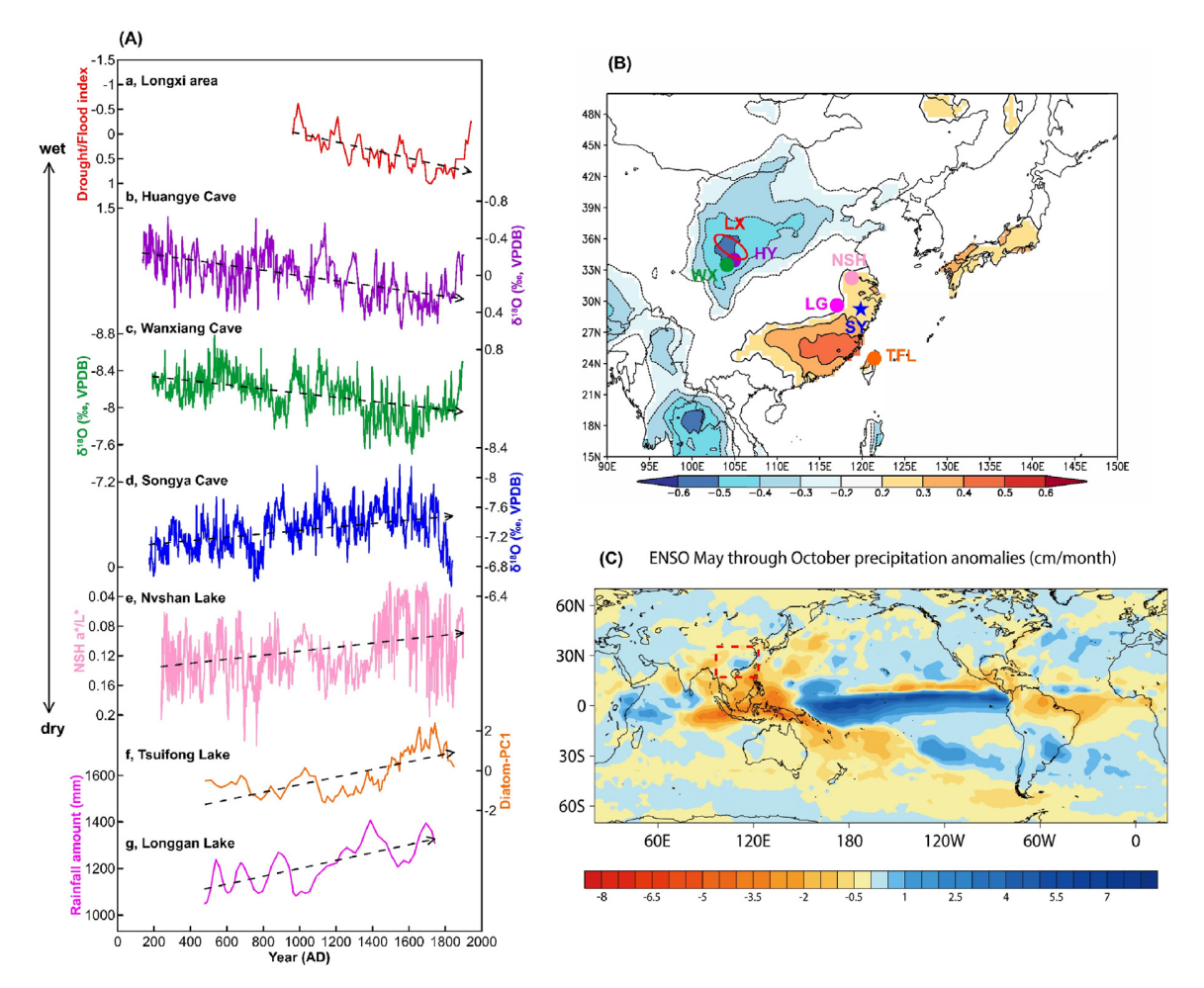


Fig. 6. (A) Comparison of EASM rainfall reconstructions from northwestern and southeastern China over the last two millennia. (a) Drought/flood index from Longxi (Tan et al., 2008). (b) Stalagmite  $\delta^{18}$ O record from Wanxiang Cave (Zhang et al., 2008). (d) Stalagmite  $\delta^{18}$ O record from Songya Cave (this study). (e) Precipitation record from lightness-normalized red color from Nvshan Lake (Jiang et al., 2021). (f) Principal component of diatom species from Tsuifong Lake (Wang et al., 2013). (g) Pollen-reconstructed rainfall from Longgan Lake (Tong et al., 1997). The black dashed lines represent the liner fitting results of these paleo-rainfall records. (B) Correlation map (modified from Lu et al., 2019) for Niño3 relative index with CRUTS4.0 gridded  $(0.5^{\circ} \times 0.5^{\circ})$  precipitation fields during the period of 1950–2018 (Harris et al., 2014). Colored contours represent the correlation coefficients (p < 0.01) between El Niño and precipitation. (C) Map of precipitation anomalies (May–October, cm/month) during the El Niño years of 1979-2006AD (data source: http://research.jisao.washington.edu/data/gpcp/). The red dotted rectangle denotes the location of study area. (For interpretation of the references to color in this figure legend, the reader is referred to the Web version of this article.)

1979-2006AD (Fig. 6C). Therefore, both proxy comparisons and meteorological studies support the view that ENSO modulates the anti-phased rainfall pattern between southeastern and northwestern China. During the El Niño-like conditions (positive phase of PDO), the intensified and southward WPSH, leads to more moisture delivery to southeastern China and less delivery to northwestern China. In contrast, during the La Niña-like conditions (negative phase of PDO), the weakened and northeastward WPSH, results in more water vapor delivered to the EASM limit regions (Zhou and Yu, 2005; Yang et al., 2017), causing dry condition in southeastern China and wet condition in northwestern China. Our finding is also supported by the width and carbon isotope records of tree-ring (Gu Mountain) in Fujian Province, suggesting that the northward shift of the monsoon rain belt induced hot and dry climate in southeastern China during La Niña episodes (Bai et al., 2021).

Additionally, the "southeastern-northwestern" diploe rainfall pattern may be related to different moisture contribution from the Indian Ocean and Pacific Ocean (Zhou and Yu, 2005; Wang and Chen, 2012). As shown in Fig. 1A, summer wind field shows that

monsoon rainfall in southeastern China is mainly from the tropical western Pacific and monsoon rainfall in northwestern China is primarily derived from the Indian Ocean. Multi-year mean air mass backward trajectories at the Songya Cave also indicate that ~47% of the water vapor is derived from the tropical western Pacific (Fig. 1B). For the Wanxiang cave, as the only source of tropical moisture, the Indian Ocean contributes ~23% moisture and South China Sea contributes ~16% moisture (Fig. S6). Therefore, the southeastern China is dominated by the EASM (the second branch of tropical water vapor), and the northwestern China is mainly controlled by ISM (the first branch of tropical water vapor). This result is supported by a high similarity of  $\delta^{18}$ O records from the Wanxiang and Dandak Cave (Berkelhammer et al., 2010; Fig. S7). The Dandak  $\delta^{18}$ O record exhibits a strong correlation with the ISM rainfall amount (Sinha et al., 2007).

Moreover, numerous geographical records have shown that the Asian summer monsoon (ASM) has strengthened over the past two millennia in an anomalous fashion relative to the decreasing trend in Northern Hemisphere summer insolation, namely the '2-kyr shift' (Cheng et al., 2016; Zhao et al., 2021). In Fig. 6A, the '2-kyr

**Table 1**Hydroclimate records mentioned in Fig. 1.

Code	Area	Site name	Туре	Latitude	Longitude	Reference
SY	Southeastern China	Songya Cave	Stalagmite	29°10′N	119°40′E	this study
LG	Southeastern China	Longgan Lake	Lake	~29°50′-30°05′N	115°55′-116°20′E	Tong et al. (1997)
NSH	Southeastern China	Nvshan Lake	Lake	32°59′N	118°07′E	Jiang et al. (2021)
TFL	Southeastern China	Tsuifong Lake	Lake	24°30′N	121°26′E	Wang et al. (2013)
JN	Southeastern China	Jiangnan area	Historical documents	~25°00′-31°00′N	East of 105°00'E	Zheng et al. (2006)
GM	Southeastern China	Gu Mountains	Tree-ring	~25°53′-26°03′N	119°60′-119°24′E	Bai et al. (2021)
MD	The East China Sea	MD05-2908 Core	Marine Core	24°48′N	122°29′E	Li et al. (2011)
WX	Northwestern China	Wanxiang Cave	Stalagmite	33°19′N	105°00′E	Zhang et al. (2008)
HY	Northwestern China	Huangye Cave	Stalagmite	33°35′N	105°07′E	Tan et al. (2011)
DY	Northwestern China	Dayu Cave	Stalagmite	33°08′N	106° 18′ E	Tan et al. (2009)
LX	Northwestern China	Longxi area	Historical documents	~34°30′-36°30′N	103°30′-106°00′E	Tan et al. (2008)
HS	Central China	Heshang Cave	Stalagmite	30°27′N	110°25′E	Hu et al. (2008)
SQ	Southwestern China	Shenqi Cave	Stalagmite	28°56′N	103°06′E	Tan et al. (2018)
DG	Southwestern China	Dongge Cave	Stalagmite	25°17′N	108°50′E	Duan et al. (2014)
Sahiya	Indian	Sahiya Cave	Stalagmite	30°36′N	77°52′E	Sinha et al. (2015)
Dandak	Central India	Dandak Cave	Stalagmite	19°00′N	82°00′E	Berkelhammer et al. (2010)
Klang	Thailand	Klang Cave	Stalagmite	8°20′N	98°44′E	Tan et al. (2019)

shift' is characterized by a decreased trend in SY6  $\delta^{18}$ O values in southeastern China but an increased trend in Wanxiang and Huangye  $\delta^{18}$ O values in northwestern China. The long-term trends in  $\delta^{18}$ O records from Shenqi Cave (southwestern China, Tan et al., 2018) and Heshang Cave (central China, Hu et al., 2008) are positively linked to WX42B record, but negatively related to the SY6 record (Fig. S8). The increased trend in stalagmite  $\delta^{18}$ O values over the past two millennia was also reported in Klang Cave from the northern tropics (Thailand), where the ISM delivers >75% of the annual rainfall from the Indian Ocean (Tan et al., 2019; Fig. S8). Besides, the '2-kyr shift' is rather flat in stalagmite record from Dongge Cave (southwestern China, Duan et al., 2014) and Sahiya Cave (Indian, Sinha et al., 2015) (Fig. S8). The regional differences in the '2-kyr shift' can also be explained by the different moisture contribution from Pacific Ocean and Indian Ocean.

During boreal summer, ISM enters into China through the "water vapor channel" (the first branch of tropical water vapor) along the southeastern edge of the Tibetan plateau and moves northwards along southwestern, central and northwestern China (Fig. 1). Thus, summer rainfall in southwestern and northwestern China is primarily derived from the Indian Ocean, but the southeastern China is dominated by the moisture form Pacific Ocean. During the El Niño-like condition, the weakened ISM results in less water vapor from the Indian Ocean delivered to the monsoonal China, especially the northwestern China. At the same time, the enhanced and southward WPSH regulates more water vapor from the tropical western Pacific to the southeastern China. During the La Niña-like condition, the enhanced ISM contributes more water vapor to the northwestern China. The weakened and northeastward WPSH leads to the Summer Drought over southeastern China. Therefore, ENSO plays an important role in modulating the spatiotemporal rainfall pattern in eastern China, probably through the rainfall amount effect and moisture source effect.

In conclusion, both "amount effect" and "source effect" can affect the spatial rainfall pattern in EASM domain on various timescales. However, knowledge of the spatiotemporal pattern of EASM rainfall remains challenging, such as the difference between the stalagmite records from Dayu Cave and Wanxiang Cave (only 120 km between them) over the past 750 years (Tan et al., 2009). This regional difference could be caused by either climatic (orographic rain, albedo and/or evapotranspiration) or non-climatic (complexity of karst system and/or uncertainty from dating and signal/noise ratio) origins. Hence, more high-quality hydroclimate reconstructions and modelling studies are needed to better understand the spatial pattern of EASM rainfall. Table 1.

#### 5. Conclusion

Here we present a ~3 year-resolution EASM rainfall record over the past two millennia, based on 13  $^{230}\text{Th}$  dates and 600  $\delta^{18}\text{O}$  measurements in a stalagmite (SY6) from Songya Cave, southeastern China. The main conclusions are as follows:

- 1) The SY6  $\delta^{18}$ O record indicates a gradually increasing EASM rainfall over the past two millennia in southeastern China. A series of centennial-scale fluctuations are superimposed on the long-term trend. The LIA was a relatively humid period, compared with the MWP.
- 2) The long-term trend and centennial-scale oscillations in EASM rainfall changes in southeastern China are closely related to ENSO and PDO variations. The increased (decreased) EASM rainfall is correlated with El Niño-like (La Niña-like) conditions and positive (negative) phase of PDO.
- 3) Comparison of Songya and Wanxiang  $\delta^{18}$ O records reveals an anti-phased spatial rainfall pattern between southeastern and northwestern China. This "southeastern-northwestern" pattern, consistent with the longitudinal zonality in EASM rainfall pattern, is also modulated by the ENSO through changes in the location and strength of the WPSH.

#### **CRediT author statement**

K. Zhao, Y. Wang and J. Chen designed the research and experiments; J. Chen, K. Zhao and Y. Wang wrote the original manuscript. J. Chen and F. Duan collected the sample. J. Chen, Y. Liang, S. Chen, Y. Cui, C. Pian and J. Zhu performed the stable isotope analysis. J. Chen, Y. Liang, Q. Shao, H. Cheng and R.L. Edwards dated the sample. All the authors discussed the results and contributed to improve the manuscript.

#### **Declaration of competing interest**

The authors declare that they have no known competing financial interests or personal relationships that could have appeared to influence the work reported in this paper.

#### Acknowledgement

We thank Dr. Zhenqiu Zhang and Ms. Lianhua Xue for their help with the isotope analyses. This work was supported by National Natural Science Foundation of China (Grants 41931178, 42071105, 41877430, 42072207), Postgraduate Research & Practice Innovation Program of Jiangsu Province, the U.S. National Science Foundation (Grant 1702816), the Project Funded by the Priority Academic Program Development of Jiangsu Higher Education Institutions (Grant 164320H116), Jiangsu Province "Qinglan Project" (2020), the 111 Program of China (Grant D19002) and State Key Laboratory of Loess and Quaternary Geology, Institute of Earth Environment, CAS (No. SKLLQG2120).

#### Appendix A. Supplementary data

Supplementary data to this article can be found online at https://doi.org/10.1016/j.quascirev.2022.107539.

#### References

- Atwood, A.R., Sachs, J.P., 2014. Separating ITCZ- and ENSO-related rainfall changes in the Galápagos over the last 3 kyr using D/H ratios of multiple lipid biomarkers. Earth Planet Sci. Lett. 404, 408–419. https://doi.org/10.1016/ j.epsl.2014.07.038.
- Bai, M., Yao, Q., Camarero, J.J., Hu, H., Dong, Z., Li, Y., Zhou, F., Chen, X., Guo, G., Cao, X., Fang, K., 2021. El Niño-Southern Oscillation modulates insect outbreaks in humid subtropical China: evidences from tree rings and carbon isotopes. Dendrochronologia 66, 125815. https://doi.org/10.1016/j.dendro.2021.125815.
- Berkelhammer, M., Sinha, A., Mudelsee, M., Cheng, H., Edwards, R.L., Cannariato, K., 2010. Persistent multidecadal power of the Indian summer monsoon. Earth Planet Sci. Lett. 290, 166–172. https://doi.org/10.1016/j.epsl.2009.12.017.
- Chang, C.-P., Zhang, Y., Li, T., 2000. Interannual and interdecadal variations of the East asian summer monsoon and tropical pacific SSTs. Part I: roles of the subtropical ridge. J. Clim. 13, 4310–4325.
- Chen, J., Chen, F., Feng, S., Huang, W., Liu, J., Zhou, A., 2015. Hydroclimatic changes in China and surroundings during the medieval climate anomaly and little ice age: spatial patterns and possible mechanisms. Quat. Sci. Rev. 107, 98—111. https://doi.org/10.1016/j.quascirev.2014.10.012.
- Cheng, H., Edwards, R.L., Sinha, A., Spötl, C., Yi, L., Chen, S., Kelly, M., Kathayat, G., Wang, X., Li, X., Kong, X., Wang, Y., Ning, Y., Zhang, H., 2016. The Asian monsoon over the past 640,000 years and ice age terminations. Nature 534, 640–646. https://doi.org/10.1038/nature18591.
- Chiang, J.C.H., Fung, I.Y., Wu, C.-H., Cai, Y., Edman, J.P., Liu, Y., Day, J.A., Bhattacharya, T., Mondal, Y., Labrousse, C.A., 2015. Role of seasonal transitions and westerly jets in East Asian paleoclimate. Quat. Sci. Rev. 108, 111–129. https://doi.org/10.1016/j.quascirev.2014.11.009.
- Chiang, J.C.H., Swenson, L.M., Kong, W., 2017. Role of seasonal transitions and the westerlies in the interannual variability of the East Asian summer monsoon precipitation. Geophys. Res. Lett. 44, 3788–3795. https://doi.org/10.1002/ 2017GL072739.
- Conroy, J.L., Restrepo, A., Overpeck, J.T., Steinitz-Kannan, M., Cole, J.E., Bush, M.B., Colinvaux, P.A., 2009. Unprecedented recent warming of surface temperatures in the eastern tropical Pacific Ocean. Nat. Geosci. 2, 46–50. https://doi.org/10.1038/ngen390
- Cook, E.R., Anchukaitis, K.J., Buckley, B.M., D'Arrigo, R.D., Jacoby, G.C., Wright, W.E., 2010. Asian monsoon failure and megadrought during the last millennium. Science 328, 486–489. https://doi.org/10.1126/science.1185188.
- Cui, A., Ma, C., Zhao, L., Tang, L., Jia, Y., 2018. Pollen records of the little ice age humidity flip in the middle Yangtze river catchment. Quat. Sci. Rev. 193, 43–53. https://doi.org/10.1016/j.quascirev.2018.06.015.
- Dayem, K.E., Molnar, P., Battisti, D.S., Roe, G.H., 2010. Lessons learned from oxygen isotopes in modern precipitation applied to interpretation of speleothem records of paleoclimate from eastern Asia. Earth Planet Sci. Lett. 295, 219–230. https://doi.org/10.1016/j.epsl.2010.04.003.
- Ding, Y., Chan, Johnny C.L., 2005. The East Asian summer monsoon: an overview. Meteorol. Atmos. Phys. 89, 117–142. https://doi.org/10.1007/s00703-005-0125-
- Ding, Y., Sun, Y., Wang, Z., Zhu, Y., Song, Y., 2009. Inter-decadal variation of the summer precipitation in China and its association with decreasing Asian summer monsoon Part II: possible causes. Int. J. Climatol. 29, 1926–1944. https://doi.org/10.1002/ioc.1759.
- Ding, Y., Wang, Z., Sun, Y., 2008. Inter-decadal variation of the summer precipitation in East China and its association with decreasing Asian summer monsoon. Part I: observed evidences. Int. J. Climatol. 28, 1139–1161. https://doi.org/10.1002/ joc.1615.
- Dong, B., Dai, A., 2015. The influence of the interdecadal pacific oscillation on temperature and precipitation over the globe. Clim. Dynam. 45, 2667–2681. https://doi.org/10.1007/s00382-015-2500-x.
- Draxler, R., Hess, G., 1998. An overview of the HYSPLIT\_4 modeling system for trajectories, dispersion, and deposition. Aust. Meteorol. Mag. 47, 295–308.
- Duan, F., Wang, Y., Shen, C.-C., Wang, Yi, Cheng, H., Wu, C.-C., Hu, H.-M., Kong, X., Liu, D., Zhao, K., 2014. Evidence for solar cycles in a late Holocene speleothem record from Dongge Cave, China. Sci. Rep. 4, 5159. https://doi.org/10.1038/

srep05159.

- Duan, W., Ruan, J., Luo, W., Li, T., Tian, L., Zeng, G., Zhang, D., Bai, Y., Li, J., Tao, T., Zhang, P., Baker, A., Tan, M., 2016. The transfer of seasonal isotopic variability between precipitation and drip water at eight caves in the monsoon regions of China. Geochem. Cosmochim. Acta 183, 250–266. https://doi.org/10.1016/j.gca.2016.03.037.
- Fang, K., Chen, D., Ilvonen, L., Pasanen, L., Holmström, L., Seppä, H., Huang, G., Ou, T., Linderholm, H., 2019. Oceanic and atmospheric modes in the pacific and atlantic oceans since the little ice age (LIA): towards a synthesis. Quat. Sci. Rev. 215, 293–307. https://doi.org/10.1016/j.quascirev.2019.05.014.Harris, I., Jones, P.D., Osborn, T.J., Lister, D.H., 2014. Updated high-resolution grids of
- Harris, I., Jones, P.D., Osborn, T.J., Lister, D.H., 2014. Updated high-resolution grids of monthly climatic observations — the CRU TS3.10 Dataset. Int. J. Climatol. 34, 623—642. https://doi.org/10.1002/joc.3711.
- Hendy, C.H., 1971. The isotopic geochemistry of speleothems—I. The calculation of the effects of different modes of formation on the isotopic composition of speleothems and their applicability as palaeoclimatic indicators. Geochem. Cosmochim. Acta 35, 801–824. https://doi.org/10.1016/0016-7037(71)90127-X.
- Hercman, H., Pawlak, J., 2012. MOD-AGE: an age-depth model construction algorithm. Quat. Geochronol. 12, 1–10. https://doi.org/10.1016/j.quageo.2012.05.003.
- Hu, C., Henderson, G.M., Huang, J., Xie, S., Sun, Y., Johnson, K.R., 2008. Quantification of Holocene Asian monsoon rainfall from spatially separated cave records. Earth Planet Sci. Lett. 266, 221–232. https://doi.org/10.1016/j.epsl.2007.10.015.
- Jiang, S., Zhou, X., Sachs, J.P., Luo, W., Tu, L., Liu, X., Zeng, L., Peng, S., Yan, Q., Liu, F., Zheng, J., Zhang, J., Shen, Y., 2021. Central eastern China hydrological changes and ENSO-like variability over the past 1800 yr. Geology. https://doi.org/ 10.1130/G48894.1.
- Lamb, H., 1965. The early medieval warm epoch and its sequel. Palaeogeogr. Palaeoclimatol. Palaeoecol. 1. 13—37.
- Li, D., Jiang, H., Li, T., Zhao, M., 2011. Late Holocene paleoenvironmental changes in the southern Okinawa Trough inferred from a diatom record. Chin. Sci. Bull. 56, 1131. https://doi.org/10.1007/s11434-011-4369-3.
- Lu, F., Ma, C., Zhu, C., Lu, H., Zhang, X., Huang, K., Guo, T., Li, K., Li, L., Li, B., Zhang, W., 2019. Variability of East Asian summer monsoon precipitation during the Holocene and possible forcing mechanisms. Clim. Dynam. 52, 969–989. https:// doi.org/10.1007/s00382-018-4175-6
- MacDonald, G.M., Case, R.A., 2005. Variations in the pacific decadal oscillation over the past millennium. Geophys. Res. Lett. 32. https://doi.org/10.1029/ 2005G1022478.
- Mann, M.E., Zhang, Z., Rutherford, S., Bradley, R.S., Hughes, M.K., Shindell, D., Ammann, C., Faluvegi, C., Ni, F., 2009. Global signatures and dynamical origins of the little ice age and medieval climate anomaly. Science 326, 1256–1260. https://doi.org/10.1126/science.1177303.
- Mantua, N.J., Hare, S.R., Zhang, Y., Wallace, J.M., Francis, R.C., 1997. A pacific interdecadal climate oscillation with impacts on salmon production. Bull. Am. Meteorol. Soc. 78, 1069–1080.
- Masson-Delmotte, V., Schulz, M., Abe-Ouchi, A., Beer, J., Ganopolski, A., González Rouco, J.F., Jansen, E., Lambeck, K., Luterbacher, J., Naish, T.R., Osborn, T., Otto-Bliesner, B.L., Quinn, T.M., Ramesh, R., Rojas, M., Shao, X., Timmermann, A., 2013. Information from Paleoclimate Archives. https://doi.org/10.1594/PANGAEA.828636.
- Matsumura, S., Horinouchi, T., 2016. Pacific Ocean decadal forcing of long-term changes in the western Pacific subtropical high. Sci. Rep. 6, 37765. https:// doi.org/10.1038/srep37765.
- Rustic, G.T., Koutavas, A., Marchitto, T.M., Linsley, B.K., 2015. Dynamical excitation of the tropical Pacific Ocean and ENSO variability by little ice age cooling. Science 350, 1537–1541. https://doi.org/10.1126/science.aac9937.
- Shao, Q., Pons-Branchu, E., Zhu, Q., Wang, W., Valladas, H., Fontugne, M., 2017. High precision U/Th dating of the rock paintings at Mt. Huashan, Guangxi, southern China. Quat. Res. 88, 1–13. https://doi.org/10.1017/qua.2017.24.
- Sinha, A., Cannariato, K.G., Stott, L.D., Cheng, H., Edwards, R.L., Yadava, M.G., Ramesh, R., Singh, I.B., 2007. A 900-year (600 to 1500 A.D.) record of the Indian summer monsoon precipitation from the core monsoon zone of India. Geophys. Res. Lett. 34. https://doi.org/10.1029/2007GL030431.
- Sinha, A., Kathayat, G., Cheng, H., Breitenbach, S.F.M., Berkelhammer, M., Mudelsee, M., Biswas, J., Edwards, R.L., 2015. Trends and oscillations in the Indian summer monsoon rainfall over the last two millennia. Nat. Commun. 6, 6309. https://doi.org/10.1038/ncomms/309
- 6309. https://doi.org/10.1038/ncomms7309.

  Tan, L., Cai, Y., Yi, L., An, Z.S., Li, A., 2008. Precipitation variations of Longxi, northeast margin of Tibetan Plateau since AD 960 and their relationship with solar activity. Clim. Past 4, 19–28. https://doi.org/10.5194/cp-4-19-2008.
- Tan, L., Cai, Y., Cheng, H., An, Z., Edwards, R.L., 2009. Summer monsoon precipitation variations in central China over the past 750years derived from a highresolution absolute-dated stalagmite. Palaeogeogr. Palaeoclimatol. Palaeoecol. 280, 432–439. https://doi.org/10.1016/j.palaeo.2009.06.030.
- Tan, L., Cai, Y., An, Z., Edwards, R., Cheng, H., Shen, C.-C., Zhang, H., 2011. Centennial to decadal-scale monsoon precipitation variability in the semi-humid region, northern China during the last 1860 years: records from stalagmites in Huangye Cave. Holocene 21, 287–296. https://doi.org/10.1177/0959683610378880.
- Tan, L., Cai, Y., Cheng, H., Edwards, L.R., Lan, J., Zhang, H., Li, D., Ma, L., Zhao, P., Gao, Y., 2018. High resolution monsoon precipitation changes on southeastern Tibetan Plateau over the past 2300 years. Quat. Sci. Rev. 195, 122–132. https://doi.org/10.1016/j.quascirev.2018.07.021.
- Tan, L., Shen, C.-C., Löwemark, L., Chawchai, S., Edwards, R.L., Cai, Y., Breitenbach, S.F.M., Cheng, H., Chou, Y.-C., Duerrast, H., Partin, J.W., Cai, W.,

- Chabangborn, A., Gao, Y., Kwiecien, O., Wu, C.-C., Shi, Z., Hsu, H.-H., Wohlfarth, B., 2019. Rainfall variations in central Indo-Pacific over the past 2,700 y. Proc. Natl. Acad. Sci. U.S.A. 116, 17201–17206. https://doi.org/10.1073/pnas.1903167116.
- Tan, M., 2014. Circulation effect: response of precipitation  $\delta^{18}O$  to the ENSO cycle in monsoon regions of China. Clim. Dynam. 42, 1067—1077. https://doi.org/10.1007/s00382-013-1732-x.
- Tong, G., Shi, Y., Wu, R., Yang, X., Zhai, W., 1997. Vegetation and climatic quantitative reconstruction of Longgan Lake since the past 3000 year. Mar. Geol. Quat. Geol. 17, 54–62 (in Chinese with English abstract).
- Wang, H., Chen, H., 2012. Climate control for southeastern China moisture and precipitation: Indian or East Asian monsoon? J. Geophys. Res. Atmos. 117, 12109. https://doi.org/10.1029/2012/D017734.
- Wang, L.-C., Behling, H., Lee, T.-Q., Li, H.-C., Huh, C.-A., Shiau, L.-J., Chen, S.-H., Wu, J.-T., 2013. Increased precipitation during the Little Ice Age in northern Taiwan inferred from diatoms and geochemistry in a sediment core from a subalpine lake. J. Paleolimnol. 49. https://doi.org/10.1007/s10933-013-9679-9.
- Yang, Q., Ma, Z., Fan, X., Yang, Z.-L., Xu, Z., Wu, P., 2017. Decadal modulation of precipitation patterns over eastern China by sea surface temperature anomalies. J. Clim. 30, 7017–7033. https://doi.org/10.1175/JCLI-D-16-0793.1.
- Yao, Y., Yang, H., Liu, W., Li, X., Chen, Y., 2015. Hydrological changes of the past 1400 years recorded in δD of sedimentary n-alkanes from Poyang Lake, southeastern China. Holocene 25, 1068−1075. https://doi.org/10.1177/0959683615576231.
- Yoshimura, K., Kanamitsu, M., Noone, D., Oki, T., 2008. Historical isotope simulation using Reanalysis atmospheric data. J. Geophys. Res. Atmos. 113. https://doi.org/ 10.1029/2008/D010074.
- Zhang, P., Cheng, H., Edwards, R.L., Chen, F., Wang, Y., Yang, X., Liu, J., Tan, M., Wang, X., Liu, J., An, C., Dai, Z., Zhou, J., Zhang, D., Jia, J., Jin, L., Johnson, K.R.,

- 2008. A test of climate, sun, and culture relationships from an 1810-year Chinese cave record. Science 322, 940–942. https://doi.org/10.1126/science 1163965
- Zhang, H., Cheng, H., Sinha, A., Spötl, C., Cai, Y., Liu, B., Kathayat, G., Li, H., Tian, Y., Li, Y., Zhao, J., Sha, L., Lu, J., Meng, B., Niu, X., Dong, X., Liang, Z., Zong, B., Ning, Y., Lan, J., Edwards, R.L., 2021a. Collapse of the Liangzhu and other Neolithic cultures in the lower Yangtze region in response to climate change. Sci. Adv. 7, eabi9275. https://doi.org/10.1126/sciadv.abi9275.
- Zhang, J., Zhao, K., Wang, Y., Kong, X., Shao, X., Liang, Y., Cui, Y., Cheng, H., Edwards, R.L., Shao, Q., 2021b. Modulation of centennial-scale hydroclimate variations in the middle Yangtze River Valley by the East Asian-Pacific pattern and ENSO over the past two millennia. Earth Planet Sci. Lett. 576, 117220. https://doi.org/10.1016/j.epsl.2021.117220.
- Zhao, J., Tan, L., Yang, Y., Pérez-Mejías, C., Brahim, Y.A., Lan, J., Wang, J., Li, H., Wang, T., Zhang, H., Cheng, H., 2021. New insights towards an integrated understanding of NE Asian monsoon during mid to late Holocene. Quat. Sci. Rev. 254, 106793. https://doi.org/10.1016/j.quascirev.2020.106793.
- Zhao, K., Wang, Y., Edwards, R.L., Cheng, H., Kong, X., Liu, D., Shao, Q., Cui, Y., Huang, C., Ning, Y., Yang, X., 2020. Late Holocene monsoon precipitation changes in southern China and their linkage to Northern Hemisphere temperature. Quat. Sci. Rev. 232, 106191. https://doi.org/10.1016/j.quascirev.2020.106191.
- Zheng, J., Wang, W.-C., Ge, Q., Man, Z., Zhang, P., 2006. Precipitation variability and extreme events in eastern China during the past 1500 years. Terr. Atmos. Ocean Sci. 17. https://doi.org/10.3319/TAO.2006.17.3.579(A).
- Zhou, T.-J., Yu, R.-C., 2005. Atmospheric water vapor transport associated with typical anomalous summer rainfall patterns in China. J. Geophys. Res. Atmos. 110, D08104. https://doi.org/10.1029/2004JD005413.